

Journal Pre-proof

2D-titanium carbide (MXene) based selective electrochemical sensor for simultaneous detection of ascorbic acid, dopamine and uric acid

N. Murugan, R. Jerome, M. Preethika, Anandhakumar
Sundaramurthy, Ashok K. Sundramoorthy



PII: S1005-0302(20)30813-6

DOI: <https://doi.org/10.1016/j.jmst.2020.07.037>

Reference: JMST 2555

To appear in: *Journal of Materials Science & Technology*

Received Date: 29 March 2020

Revised Date: 17 June 2020

Accepted Date: 13 July 2020

Please cite this article as: { doi: <https://doi.org/>

This is a PDF file of an article that has undergone enhancements after acceptance, such as the addition of a cover page and metadata, and formatting for readability, but it is not yet the definitive version of record. This version will undergo additional copyediting, typesetting and review before it is published in its final form, but we are providing this version to give early visibility of the article. Please note that, during the production process, errors may be discovered which could affect the content, and all legal disclaimers that apply to the journal pertain.

© 2020 Published by Elsevier.

Research Article

2D-titanium carbide (MXene) based selective electrochemical sensor for simultaneous detection of ascorbic acid, dopamine and uric acid

N. Murugan ^{a,±}, R. Jerome ^{a,±}, M. Preethika ^a, Anandhakumar Sundaramurthy^b, Ashok K. Sundramoorthy ^{a,*}

^a Department of Chemistry, SRM Institute of Science and Technology, Kattankulathur-603 203, Tamil Nadu, India

^b SRM Research Institute, SRM Institute of Science and Technology, Kattankulathur-603 203, Tamil Nadu, India

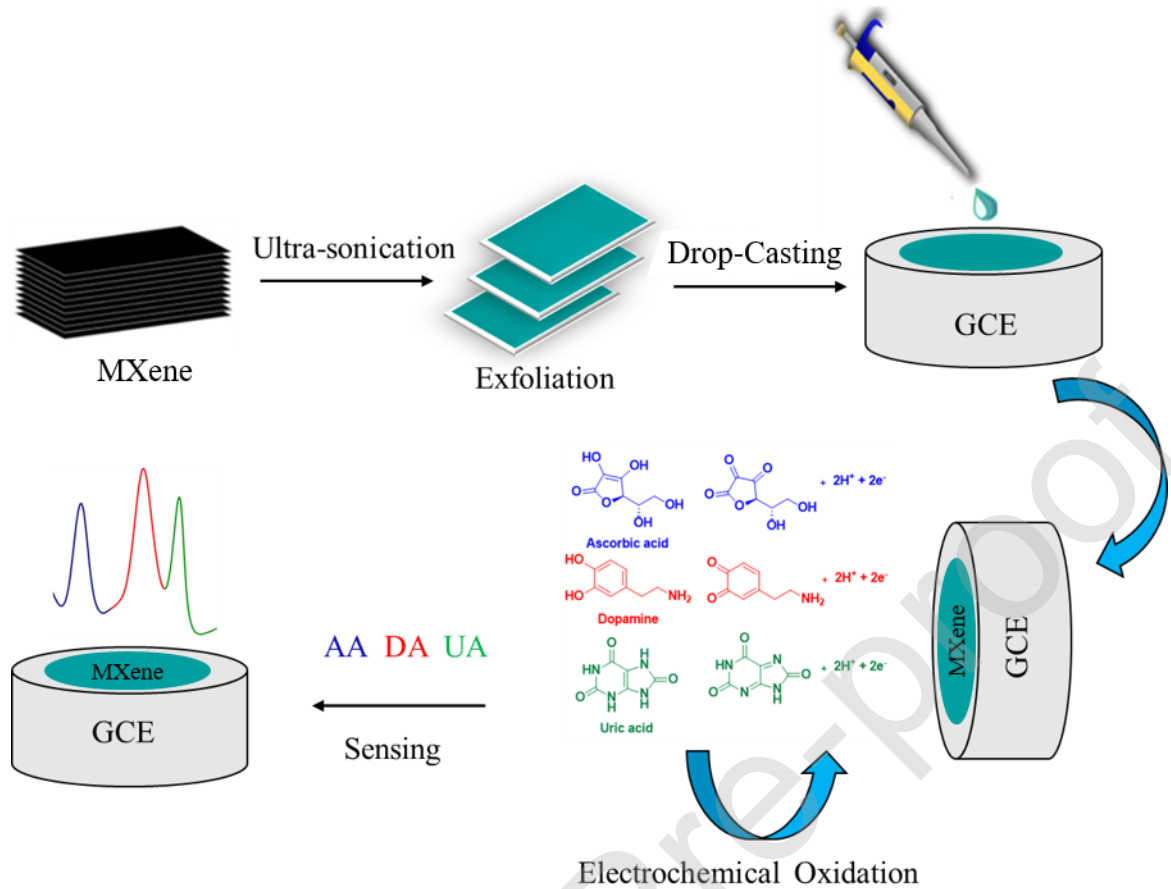
*Corresponding author.

[±]These authors contributed equally to this work.

E-mail address: ashokkus@srmist.edu.in (Ashok K. Sundramoorthy).

[Received 29 March 2020; Received in revised form 17 June 2020; Accepted 13 July 2020]

Graphical Abstract



Abstract

Two-dimensional (2D) titanium carbide (MXene) nanosheets exhibited excellent conductivity, flexibility, high volumetric capacity, hydrophilic surface, thermal stability, etc. So, it has been exploited in various applications. Herein, we report synthesis of mixed phase 2D MXene as a catalytic material for simultaneous detection of important biomolecules such as ascorbic acid (AA), dopamine (DA) and uric acid (UA). Crystalline structure, surface morphology and elemental composition of mixed phase titanium carbide (Ti-C-T_x) MXene ($T_x = -\text{F}, -\text{OH}, \text{ or } -\text{O}$) nanosheets were confirmed by X-ray diffraction (XRD), Raman spectroscopy,

high-resolution transmission electron microscopy (HR-TEM), high-resolution scanning electron microscopy (HR-SEM) and Energy-dispersive X-ray spectroscopy (EDS) mapping analysis. Furthermore, Ti-C-T_x modified glassy carbon electrode (GCE) was prepared and its electrochemical properties are studied by cyclic voltammetry (CV) and differential pulse voltammetry (DPV). It was found that Ti-C-T_x modified GCE (Ti-C-T_x/GCE) showed excellent electrocatalytic activity and separated oxidation peaks of important biomolecules such as AA (at 0.01 V), DA (at 0.2 V) and UA (at 0.33 V). Also, Ti-C-T_x/GCE sensor is enabled their simultaneous detection in physiological pH from 100 - 1000 μM for AA, 5 - 50 μM for DA and 0.5 – 4 μM & 100 - 1500 μM for UA. The limit of detection's (LOD) was estimated as 4.6 μM, 0.06 μM and 0.075 μM for AA, DA and UA, respectively. Moreover, real sample analysis indicated that spiked AA, DA and UA can be determined accurately by Ti-C-T_x/GCE with the recovery ratio in the range between 101.5% to 103% in human urine samples. The proposed Ti-C-T_x modified electrode exhibited good stability, selectivity and reproducibility as an electrochemical sensor for the detection of AA, DA and UA molecules.

Keywords: Titanium carbide; Dopamine; Uric acid; Ascorbic acid; Electrochemical sensor

1. Introduction

Two-dimensional (2D) layered materials are receiving great attention in the past few years because of their unique physicochemical properties, fast electron transfers kinetics, planer structure, wide surface area, desirable surface tunability, minimal layer thickness and high electrical conductivity. These layered nanostructures have been utilized in the construction of electrochemical biosensors, surface Plasmon resonance (SPR) sensor, energy storage devices, cancer therapy, drug delivery, etc[1–6]. Similarly, refractive index sensor is also fabricated using

a microfiber Bragg grating with a KrF excimer laser in a highly Ge-doped photosensitive microfiber [7], MoO₃ nanobelts based trimethylamine gas sensor [8] and carbon nanotube based healable transparent chemical gas sensor were reported [9].

Recently, 2D titanium carbide (MXene) nanosheets have been emerged as a crucial material to construct highly sensitive biosensors devices due to its large hydrophilic surface, low framework density, high electrochemical performances, and good electrical conductivity which favors their potential applications in electrochemistry[10,11]. Compared to graphene, MXene possess high conductivity (9880 S cm^{-1})[12], high Young's modulus ($333\pm30 \text{ GPa}$)[13] and high water flux ($85.4 \text{ Lm}^{-2} \text{ h}^{-1}$) with excellent salt rejection (~99.5%) properties [14]. In addition, MXenes are more promising than other 2D materials due to its strong interaction between Ti and C bond. Generally, two common methods are available to synthesize 2D materials such as chemical vapor deposition (CVD), and top-down approach[15]. For example, Xu et al. used CVD method to produce thin Mo₂C, WC and TaC films[16]. In the top-down approach, layered materials are obtained from the bulk solids by various exfoliation methods [13,17]. Compared to several other synthesis methods, top-down and bottom-up methods are usually utilized to prepare MXenes with single, few, or multilayer sheets[18–22].

As-synthesized MXene possess excellent electrical conductivity, good ion-intercalation behavior, easy functionalization, high hydrophilicity (due to -OH, -O and -F) (verified by water droplet contact analysis, Fig. S1 in Supplementary File), large scale production, some organic solubility, faster access to analyte, etc. which made MXene as a perfect material to fabricate high performance electrochemical (bio) sensors [18,23,24]. Recently, multi-dimensional nanostructure constructed by self-reduction of bimetallic nanoparticles (Au-Pd NPs) on the

exterior of ultrathin MXene ($Ti_3C_2T_x$) nanosheets was used to immobilize acetylcholinesterase enzyme to detect paraoxon pesticide in agricultural products[25]. This MXene/Au-Pd sensor showed good electron transfer, high sensitivity, superior conductivity and stability during the detection of pesticide. Zhang et al. fabricated the MXene based screen-printed electrode for the determination of acetaminophen and isoniazid in 0.1 M H_2SO_4 , which exhibited good sensitivity and stability for drug monitoring[26]. Moreover, the MXene based electrochemical microfluidic biosensor is also constructed to monitor the uric acid, urea, and creatinine in whole blood with good sensitivity and stability [27]. The alk- Ti_3C_2 modified GCE has been used for simultaneous detection of Cd(II), Pb(II), Cu(II) and Hg(II) ions [28]. Bio-functionalized Ti_3C_2 is also used for ultrasensitive detection of cancer biomarker[29] and glucose[30].

On the other hand, the elevated level of biomolecules such as dopamine (DA), uric acid (UA) and ascorbic acid (AA) are highly responsible for several major human health problems[31]. DA is an important catecholamine neurotransmitter of the central nervous system; particularly DA concentration is measured in the range from 10 nM – 1 μM in biological system[32]. The abnormal level of DA in biological fluids is an indicator for numerous neurological diseases such as Parkinson's disease, schizophrenia, hormonal cardiovascular systems and HIV infection[33]. Similarly, UA is an end product of purine metabolism as it found in the range between 207 – 444 μM in human body. The increased or inadequate level of UA could cause several illnesses such as kidney failure, gout, cardiovascular and chronic renal sickness, pneumonia, hyperuricemia, etc [34,35]. In addition, AA is one of the most essential vitamin in human body due to their antioxidant properties. It acts as a protective agent of cells/tissues from oxidative stress and plays a great performance in the metabolic process of

human body [36,37]. The intracellular concentration of AA is estimated as 1 – 2 mM in normal condition, an unusual level of AA is causing several illnesses in human central nervous system. Generally, AA concentration is higher than the concentrations of DA and UA in biological systems [38,39]. Hence, the rapid and accurate measurements of AA, DA and UA concentrations in biological fluids are necessary for clinical diagnosis of relevant diseases. The electrochemical detection methods have been widely used to detect AA, DA and UA in biological matrix. However, many of the sensors failed to detect accurately each individual molecules due to their co-existence (AA, DA and UA) in real biological samples and their overlapping oxidation potentials [40,41]. Furthermore, bare working electrode could result in poor resolution, stability, linear range and inaccurate determination of DA. Interestingly, the aforementioned problems can be solved by using modified electrochemical sensor due to its outstanding features such as highly sensitive, label-free, rapid response, and selective detection [42–47]. Recently, electrochemical sensors such as 3,4,9,10-perylenetetracarboxylic acid and l-cysteine deposited gold nanocrystals modified electrode [48], ZnO nanosheets and copper oxide decorated polypyrrole nanofibers modified electrode [49], hexadecyl trimethyl ammonium bromide functionalized graphene oxide/multiwalled carbon nanotubes modified GCE [50], reduced graphene oxide functionalized poly(amido-amine)/multi-walled carbon nanotubes/gold nanoparticles modified GCE [51], palladium nanoparticles deposited graphitized carbon monolith modified electrode [52] and graphene oxide-based nanomaterials were reported for the simultaneous detection of AA, DA and UA [42,53]. However, some of these sensors have limitations such as complicated electrode fabrication process, involving extensive processing steps, associated high cost and instability.

Herein, we have demonstrated an effective electrochemical sensor using Ti-C- T_x (MXene) nanosheet modified electrode for simultaneous detection of biomolecules. The physiochemical features and electrochemical performances of formulated Ti-C- T_x (MXene) nanosheets were confirmed by a diverse characterization studies such as X-ray diffraction (XRD), Raman spectroscopy, high-resolution transmission electron microscopy (HR-TEM), high-resolution scanning electron microscopy (HR-SEM) and EDS mapping analysis. Furthermore, Ti-C- T_x modified glassy carbon electrode (Ti-C- T_x /GCE) was prepared and its electrochemical properties are studied by cyclic voltammetry (CV) and differential pulse voltammetry (DPV) in 0.1 M PBS (pH 7.4). Effect of scan rate (from 10 to 150 mV s⁻¹) on the oxidation peak currents of AA, DA and UA is recorded by CV in 0.1 M PBS. The Ti-C- T_x /GCE exhibited a linear response toward AA, DA and UA in the range of 100 – 1000 µM, 10 – 50 µM and 100 – 1500 µM, respectively. Moreover, spiked AA, DA and UA in human urine sample was analyzed by Ti-C- T_x /GCE and found that the recovery values were from 101.5% to 103%. In addition, the proposed Ti-C-Tx modified electrode exhibited excellent stability, selectivity, reproducibility and repeatability.

2. Experimental

2.1. Chemicals and reagents

Titanium metal powder (325 mesh), aluminum metal powder (325 mesh), graphite nanopowder (400 nm), sodium dihydrogen phosphate monohydrate (H₂NaO₄P.H₂O), hydrofluoric acid (40% HF), sodium phosphate dibasic heptahydrate (Na₂HPO₄.7H₂O), AA, DA, nicotine, l-cysteine, paracetamol and UA were purchased from Alfa Aesar and Sigma-Aldrich

(used without further purifications). Cadmium chloride (CdCl_2) and lead sulfate (PbSO_4) were purchased from Avra Laboratories Private Limited, Hyderabad, India.

2.2. Synthesis of Ti-C-T_x powders

The Ti-C-T_x MXene was formulated by the self-propagating high-temperature route under N_2 environment. Powder forms of Ti, Al and C were (precursors) mixed at mass ratio of 3:1:2 and grinded by ball-milling for 12 h at room temperature. Then, the obtained powder was heated to 1100 °C for 2 h under N_2 atmosphere in a tubular furnace at a ramping rate of 5 °C min^{-1} . After cooling down to RT, the black color powder was collected and treated with 40% HF under constant magnetic stirring (1000 rpm) for 24 h. Finally, HF treated material was centrifuged and washed several times with distilled water (dH_2O) to neutralize their pH and dried at 70 °C using a hot air oven to get MXene powder[54].

2.3. Preparation of Ti-C-T_x modified GCE

GCE was polished using various grades of alumina (with 1.0, 0.05 and 0.3 micron) powders on micro cloth pad to get a mirror-like surface. Then, polished GCE was cleaned in water and ethanol mixture for 15 min to remove any undesirable residues by bath sonication. Finally, the GCE was rinsed three times with MilliQ water and dried. Next, 100 mg of mixed phase MXene powder was dispersed by bath sonication in 30 mL dH_2O for 1 h. Then, 10 μL of MXene suspension (3.3 mg/mL) was drop casted on GCE surface and dried overnight at RT.

2.4. Determination of DA, AA and UA in a human urine sample

To test the real application of the sensor, urine sample was collected from a healthy person (28 years old) and diluted to 1000 times using 0.1 M PBS (pH 7.4). Then, the diluted

human urine sample was spiked with known concentrations of AA, DA and UA. Finally, the recovery ratios of spiked samples are calculated.

2.5. Materials characterization

The morphological, chemical composition and surface features of synthesized MXene were investigated by high-resolution transmission electron microscopy (HR-TEM, JEM-2100 Plus, JEOL) and high-resolution scanning electron microscopy (HR-SEM) (Thermoscientific Apreo S). The crystallinity of MXene was confirmed by X-ray diffraction spectroscopy (XRD) (X'pert powder XRD system, Malvern panalytical). Raman spectrum was acquired using a Raman spectrometer (LabRAM HR evolution, Horiba) with a 532 nm excitation wavelength in the range from 100 to 2000 cm⁻¹. Energy dispersive spectroscopy (EDS) (Quanta 400 FEG, FEI) was performed for elemental and chemical composition analysis.

2.6. Electrochemical measurements

All electrochemical measurements were carried out by using CHI 760C electrochemical workstation such as CV and DPV. Three-electrode system consisting of platinum (Pt), Ti-C-T_x/GCE and Ag/AgCl (1 M KCl) were used as counter, working, and reference electrode, respectively. 0.1 M phosphate buffer solution (PBS, pH 7.4) was used as an electrolyte.

3. Results and discussion

3.1 Characterization of Ti-C-T_x (MXene)

The 2D Ti-C-T_x nanosheets were prepared by a bottom-up approach of the self-propagating high-temperature route using powder forms of three different growth precursors such as Ti, Al and C, respectively, at mass ratios of 3:1:2. Scheme 1 displays the formation process for 2D Ti-C-T_x nanosheets at different reaction conditions. The HR-SEM images of as-

synthesized 2D Ti-C- T_x displayed the layered sheet-like structures as shown in Fig. 1(A). It was clear that few layered MXene are formed by our synthesis method (Fig. 1(B)) and the thickness of the MXene film on the electrode was found to be ~180 nm. The average sizes of MXene layers are in the range from ~400 to 500 nm (Fig. 1(A) and (B)). Furthermore, elemental mapping on Ti-C- T_x nanosheet film is carried out on a selected zone by EDS (Fig. 1(C)). The elemental mapping images showed spatial distribution of Ti, C, O, and Al, respectively. Fig. 2(A) and (B) show TEM images of Ti-C- T_x MXene which exhibited a layered sheet like structure at higher magnification with the lattice spacing of approximately 0.354 nm corresponding to the standard d-spacing of Ti-C (Fig. 2(C)). Also, selected-area diffraction (SAED) pattern of MXene resulted in a well-defined diffraction rings which are indexed to mixed phases titanium carbide Ti-C- T_x . It was in good agreement with the XRD pattern as well (Fig. 3(A)).

The crystallinity nature of Ti-C- T_x was investigated by XRD. As expected, the diffraction peaks (2θ values) at 35.9° , 41.8° , 60.5° , and 72.6° are equivalent to (111), (200), (220), and (311) planes of the Ti-C- T_x , well matched with the standard JCPDS card No: 00-032-1383. XRD pattern is also showed that the peaks at 2θ values of 25.5° , 37.7° , 48.3° and 54.3° are corresponding to oxide peaks of TiO_2 and 52.5° , 57.3° and 77.0° peaks of Al_2O_3 , respectively (Fig. 3(A)). Obviously, this XRD data confirmed the formation of mixed phase titanium carbide Ti-C- T_x [55,56]. The Raman spectrum of Ti-C- T_x showed a broad band at around $\sim 153 \text{ cm}^{-1}$, corresponding to E_g vibration of TiO [57]. Moreover, the small Raman bands at $\sim 354 \text{ cm}^{-1}$ and $\sim 574 \text{ cm}^{-1}$ are assigned to the vibrations of atoms in $\text{Ti}_3\text{C}_2\text{T}_x$ [58–60]. Two additional bands observed at ~ 1336 and $\sim 1567 \text{ cm}^{-1}$, which are corresponding to D and G bands of graphitic carbon (Fig. 3(B)). These G and D bands are attributed to the vibrations of sp^2 hybridized carbon

atoms in a 2D hexagonal lattice and the presence of disordered graphitic carbon, respectively[61–63].

3.2. Electrochemical oxidation of AA, DA and UA on Ti-C-T_x modified GCE

A set of experiments was performed to determine the electrocatalytic activity of Ti-C-T_x modified GCE on the various biomolecules such as AA, DA and UA by CV in 0.1 M PBS (pH 7.4). For comparison studies, unmodified and Ti-C-T_x nanosheets modified GCE have been used to study the oxidation of individual and simultaneous detection of biomolecules such as AA (1 mM), DA (1 mM) and UA (1 mM) at a scan rate of 50 mV s⁻¹ as shown in Fig. 4. AA showed a broad oxidation peak at 0.16 V on bare GCE and this peak is shifted to (-0.03 V) on Ti-C-T_x modified GCE with significantly increased oxidation peak current ($I_{pa} = -0.8639 \mu\text{A}$) (Fig. 4(A)). The bare-GCE showed an ill-defined oxidation peak with low oxidation current ($I_{pa} = -0.1347 \mu\text{A}$) because of the lethargic electrochemical response toward AA (Fig. 4(A), red curve). Ti-C-T_x modified electrode is promoted electro-oxidation of AA compared to bare GCE. Similarly, Ti-C-T_x/GCE exhibited an excellent catalytic performance toward DA oxidation due to the high effective surface area. The oxidation and reduction peak potentials of DA were observed at (0.19 V) and (0.12 V), respectively. DA showed an oxidation peak at (0.23 V) on bare GCE, and this peak shifted to (0.19 V) on Ti-C-T_x modified GCE with increased oxidation peak current ($I_{pa} = -0.4617 \mu\text{A}$). As expected, bare GCE showed poorly defined oxidation peak with low current ($I_{pa} = -0.2538 \mu\text{A}$) for DA as shown in Fig. 4(B), red curve. Further, the reversibility of the DA's redox peak was noticeably improved on the modified electrode. In the case of UA, low oxidation peak current is observed at (0.39 V) on bare GCE, but Ti-C-T_x modified GCE is shifted the UA oxidation potential to (0.31 V) and increased UA oxidation peak current about two times

($I_{pa} = -2.987 \mu\text{A}$) compared to bare electrode ($I_{pa} = -1.042 \mu\text{A}$) (Fig. 4(C)). So, it was confirmed that Ti-C-T_x modified electrode exhibited excellent electro-catalytic effects toward AA, DA and UA.

Next, cyclic voltammograms (CVs) are recorded for a mixture of the solution containing DA (1 mM), AA (1 mM) and UA (1 mM) as shown in Fig. 4(D). At bare GCE, the oxidation peak potentials of AA, DA and UA could not be separated. But, after modified with Ti-C-T_x, the peak potentials of AA, DA and UA are clearly separated with well-defined oxidation peaks at 0.014 V, 0.21 V, 0.33 V and reduction peak of DA at 0.12 V, respectively. A distinct negative shift of AA, DA and UA oxidation peaks were noticed on Ti-C-T_x modified GCE. Due to its fast electron transfer kinetics and the synergistic effects, Ti-C-T_x modified GCE have separated the anodic peak potentials (of AA, DA, and UA) and shifted to lower potentials for each analyte compared to bare GCE. The bare GCE is showed poorly defined oxidation peaks because of the lethargic electrochemical response toward these biomolecules. In contrast, the Ti-C-T_x modified electrode is notably increased catalytic currents of AA, DA and UA compared to bare GCE. This outstanding result demonstrated that the Ti-C-T_x material had an excellent electro-catalytic effect. Furthermore, the oxidation reaction mechanisms of AA, DA and UA at Ti-C-T_x/GCE can be illustrated as shown in Fig. 5.

3.3. Effect of scan rate

The effect of scan rate on the oxidation of AA, DA and UA (each 1 mM) is studied by CV in 0.1 M PBS (pH=7.4) (Fig. 6(A-C)). The obtained results showed that oxidation peak currents increased linearly with the square root of scan rates in the range from 10 to 150 mV s⁻¹. The higher peak currents are recorded at high scan rate due to the availability of sufficient time

for accomplishing their catalytic activity towards the analyte's at the electrode surface. The oxidation peak potentials were gradually shifted to positive side which may be due to the kinetic limitation of the reaction. The linear correlation coefficient values of AA ($R^2=0.9894$), DA (I_{pa}) ($R^2=0.9639$)/(I_{pc}) ($R^2=0.9834$) and UA ($R^2=0.9865$) were calculated as shown in Fig. 6(D) and (F). So, it was confirmed that oxidation of AA, DA, and UA on Ti-C- T_x modified GCE is a diffusion-controlled process[64,65].

3.4 Individual and simultaneous measurement of AA, DA, and UA by DPV.

Figs. 7 and 8 show the differential pulse voltammograms (DPVs) of the Ti-C- T_x modified electrode for the individual and simultaneous determination of AA, DA, and UA in 0.1 M PBS (pH 7.4). Fig. 7(A-C) show the DPVs for detection of the individual molecule of AA, DA and UA at concentration ranging from 100 - 1000 μ M for AA, 5 - 50 μ M for DA and 100 -1500 μ M for UA, respectively. As the concentration of analyte increased, the oxidation peaks currents (I_{pa}) were also increased linearly. The calibration graph exhibited a good linear relationship between the peak currents *vs.* concentrations with good linear correlation coefficient values of ($R^2 = 0.9987$ for AA), ($R^2 = 0.9915$ for DA) and ($R^2 = 0.9799$ for UA) as shown in Fig. 7(D) and (F). Fig. 8(A) shows the simultaneous detection of DA and UA in a mixture solution by DPV using Ti-C- T_x modified electrode at a scan rate of 50 mV s⁻¹. It indicated a better separation of DA oxidation peak (0.13 V) from UA peak (0.25 V). A linear response was observed from 0.5 to 4 μ M for DA and 0.5 to 4 μ M for UA, respectively, with the linear correlation coefficient of $R^2 = 0.9886$ (for DA) and $R^2 = 0.9807$ (for UA) (Fig. 8(B) and (C)).

Fig. 9(A) shows the simultaneous detection of AA, DA and UA by Ti-C- T_x modified GCE which showed well-separated oxidation peaks with respect to the added concentrations

(from 100 to 600 μM for AA, 0.5 to 3 μM for DA and 0.5 to 3 μM for UA). With the concentrations of three analytes (AA, DA and UA), the oxidation peak currents (I_{pa}) are increased linearly with well-defined oxidation peak potentials at -0.1 V, 0.14 and 0.25 V for AA, DA and UA, respectively. The obtained DPVs exhibited the good linear responses for AA ($R^2 = 0.9815$), DA ($R^2 = 0.9806$) and UA ($R^2 = 0.9709$), as shown in Fig. 9(B-D). The limit of detection's (LOD) for AA, DA, and UA were calculated as 4.6 μM , 0.06 μM and 0.075 μM , respectively. LOD of AA is much higher than that of DA and UA due to its non-aromatic nature[66]. Next, the analytical performance of the proposed method is compared with the previously reported electrochemical sensors for AA, DA and UA (Table 1). It was found that our proposed sensor showed wide linear range of detection, and lowest LOD's for DA, AA and UA compared to most of the reported sensors. This improved analytical sensitivity may be ascribed to Ti-C-T_x film modified electrode and it is enhanced electro catalytic activity towards AA, DA and UA.

3.5. Real sample analysis

Practical application of the proposed Ti-C-T_x modified electrode is tested by measuring spiked AA, DA and UA in diluted human urine samples by DPV via a standard addition method. Before running the experiment, urine samples were diluted to 1000 times and spiked with known concentration of 100 μM of AA, 20 μM of DA and 100 μM of UA, respectively. Next, DPVs were recorded. From the obtained DPVs, recovery rates for AA, DA and UA were calculated as between 100.5% to 103% by triplicate measurements (Table 2). It was found that Ti-C-T_x modified GCE is a promising sensor to detect AA, DA and UA in real samples [67,68].

3.6. Reproducibility, stability and selectivity of Ti-C-T_x modified electrode

Reproducibility of the electrochemical sensor is an important indicator for the real-world applications. Reproducibility of the Ti-C- T_x modified GCE was tested for the simultaneous determination of biomolecules in 0.1 M PBS using DPV method. Reproducibility was checked out by using three different independently prepared Ti-C- T_x modified electrodes, which showed no significant changes in the oxidation peak currents for AA, DA and UA in PBS containing AA, DA and UA (each 1 mM) (Fig. 10(A)). The stability of the Ti-C- T_x /GCE was also studied. As-fabricated Ti-C- T_x /GCE was stored at ambient condition for 25 d, and the CVs are recorded in the presences of AA, DA and UA (each 1 mM) in 0.1 M PBS (pH 7.4), as shown in Fig. 10(B). This result showed that the Ti-C- T_x /GCE retained 89.6% of its initial electrochemical sensing response over 25 d even after repeated use. Next, in order to test the selectivity of the Ti-C- T_x /GCE, we conducted DPV measurements in the presence of AA (300 μ M), DA (1.5 μ M), UA (1.5 μ M). After that, DPVs are recorded again in the presence of tenfold concentrated interferent molecules such as urea, nicotine, l-cysteine, paracetamol, Cd²⁺ and Pb²⁺ in 0.1 M PBS (pH 7.4) along with AA (300 μ M), DA (1.5 μ M), UA (1.5 μ M). As shown in Fig. 10(C), the oxidation peak currents for these molecules are decreased slightly from the range of 3.7% to 6.8%. This study confirmed that these interferent compounds did not affect the selectivity of the Ti-C- T_x /GCE (Fig. 10(D)). So, it was concluded that our proposed Ti-C- T_x modified electrode had good reproducibility, stability and selectivity.

3.7. The mechanism of DA, UA and AA interactions with MXenes

The high electrochemical activity of MXene might come from its layered structure along with strong metal bonding between Ti and C atoms, which has active surface groups to improve the charge transfer between biomolecules and MXene. In addition, MXene layers are negatively

charged due to its functional groups such as ($-F$, $-OH$, or $-O$), which might be useful for accumulation of positively charged DA molecules [34]. The interactions between Ti-C- T_x /GCE and DA, UA and AA can be considered as aromatic $\pi-\pi$ stacking interactions and electrostatic interactions [43]. The electrostatic interactions between positively charged ($pK_a = 8.87$) DA and negatively charged MXene was responsible for enhanced catalytic currents at neutral pH. Also, when DA gets protonated, the positively charged ammonium cation ($-NH_3^+$) interact with the negatively charged π electrons of MXene. On the other hand, six-member heterocyclic aromatic compounds are more stable than five-member ring systems. UA has both five and six-membered aromatic rings. But, AA contains five-membered aromatic ring. So, its interaction with MXene was weaker $\pi-\pi$ stacking. Moreover, UA and AA were existed in anionic forms as urate ions (UA^-) ($pK_a = 5.4$) and ascorbate ions (AA^-) ($pK_a = 4.1$) under neutral pH. These negatively charged ions might be repelled by negatively charged MXene ($-F$, $-OH$, or $-O$) layers. But, UA can stabilize the π conjugation system through its two rings. So, UA^- has stronger $\pi-\pi$ stacking interactions with the MXene as well as H-bonding interactions between the $-NH$ of UA^- and the MXene functional groups. Also, AA might have H bonding interactions among the $-OH$ of AA^- functional groups of MXene or weaker $\pi-\pi$ interactions among AA and the MXene. So, the Ti-C- T_x /GCE possess high sensitivity towards UA compared with AA [69,70]. However, further studies are required to ascertain the detailed kinetic information on the electrochemical interaction between the MXene and these biomolecules.

4. Conclusions

We have successfully synthesized 2D (Ti-C- T_x) mixed phase MXene by facile and cost-effective one-step synthesis method. Synthesized Ti-C- T_x mixed phase MXene was characterized

by XRD, Raman spectroscopy, HR-SEM and HR-TEM. Ti-C-T_x modified GCE is successfully prepared and demonstrated for the simultaneous detection of AA, DA and UA. Remarkably, Ti-C-T_x/GCE exhibited a high sensitivity toward AA, DA and UA and the LOD's were calculated as 4.6 μM, 0.06 μM and 0.075 μM, respectively. Moreover, for real sample analysis, satisfactory recovery ratios of AA, DA and UA were observed on Ti-C-T_x/GCE from 100.5% to 103% in human urine samples. This sensor is also showed good reproducibility and linear response. Furthermore, Ti-C-T_x/GCE showed potential use as an outstanding electrochemical sensor for the simultaneous determination of AA, DA and UA in physiological pH. This study suggested that mixed phase MXene film can be used to develop real-world sensors for the detection of AA, DA and UA. We will continue to work on developing a commercial sensor devices using this material for real-world analysis and will be communicated in due course.

Acknowledgements

We acknowledge the financial support from the Science and Engineering Research Board (SERB), India (No. ECR/2016/001446) and Department of Science and Technology (International Bilateral Cooperation Division) for financial support through “INDO-RUSSIA Project (No. INT/RUS/RFBR/385)”. N. Murugan thanks the SRM-IST for the award of PDF.

References

- [1] M. Soleymaniha, M. Shahbazi, A.R. Rafieerad, A. Maleki, A. Amiri, *Adv. Health. Mater.* 8 (2019) 1801137.
- [2] J. Ji, J. Wen, Y. Shen, Y. Lv, Y. Chen, S. Liu, H. Ma, Y. Zhang, *J. Am. Chem. Soc.* 139 (2017) 11698–11701.

- [3] C. Tan, X. Cao, X.J. Wu, Q. He, J. Yang, X. Zhang, J. Chen, W. Zhao, S. Han, G.H. Nam, *Chem. Rev.* 117 (2017) 6225–6331.
- [4] J. Zhu, E. Ha, G. Zhao, Y. Zhou, D. Huang, G. Yue, L. Hu, N. Sun, Y. Wang, L.Y.S. Lee, *Coord. Chem. Rev.* 352 (2017) 306–327.
- [5] L. Wang, P. Hu, Y. Long, Z. Liu, X. He, *J. Mater. Chem. A* 5 (2017) 22855–22876.
- [6] T. Xue, W. Liang, Y. Li, Y. Sun, Y. Xiang, Y. Zhang, Z. Dai, Y. Duo, L. Wu, K. Qi, B.N. Shivananju, L. Zhang, X. Cui, H. Zhang, Q. Bao, *Nat. Commun.* 10 (2019) 28.
- [7] Y. Zhang, B. Lin, S.C. Tjin, H. Zhang, G. Wang, P. Shum, X. Zhang, *Opt. Express* 18 (2010) 26345–26350.
- [8] S. Yang, Y. Liu, W. Chen, W. Jin, J. Zhou, H. Zhang, G.S. Zakharova, *Sensors Actuat. B: Chem.* 226 (2016) 478–485.
- [9] S. Bai, C. Sun, H. Yan, X. Sun, H. Zhang, L. Luo, X. Lei, P. Wan, X. Chen, *Small* 11 (2015) 5807–5813.
- [10] J.C. Lei, X. Zhang, Z. Zhou, *Front. Phys.* 10 (2015) 276–286.
- [11] L. Ding, Y. Wei, Y. Wang, H. Chen, J. Caro, H. Wang, *Angew. Chem. Int. Edit.* 56 (2017) 1825–1829.
- [12] C. Zhang, Y. Ma, X. Zhang, S. Abdolhosseinzadeh, H. Sheng, W. Lan, A. Pakdel, J. Heier, F. Nüesch, *Energy Environ. Mater.* 3 (2020) 29–55.
- [13] M. Naguib, M. Kurtoglu, V. Presser, J. Lu, J. Niu, M. Heon, L. Hultman, Y. Gogotsi, M.W. Barsoum, *Adv. Mater.* 23 (2011) 4248–4253.
- [14] G. Liu, J. Shen, Q. Liu, G. Liu, J. Xiong, J. Yang, W. Jin, *J. Memb. Sci.* 548 (2018) 548–558.
- [15] J. Wang, G. Li, L. Li, *Two-Dimensional Materials: Charactarazation and Potential Applications*, Beijing, 2016, pp. 1–20.
- [16] C. Xu, L. Wang, Z. Liu, L. Chen, J. Guo, N. Kang, X.L. Ma, H.M. Cheng, W. Ren, *Nat. Mater.* 14 (2015) 1135–1141.
- [17] M. Alhabeb, K. Maleski, B. Anasori, P. Lelyukh, L. Clark, S. Sin, Y. Gogotsi, *Chem. Mater.* 29 (2017) 7633–7644.
- [18] M. Naguib, V.N. Mochalin, M.W. Barsoum, Y. Gogotsi, *Adv. Mater.* 26 (2014) 992–1005.
- [19] M. Khazaei, M. Arai, T. Sasaki, C. Chung, N.S. Venkataraman, M. Estili, Y. Sakka, Y. Kawazoe, *Adv. Funct. Mater.* 23 (2013) 2185–2192.

- [20] O. Mashtalir, M. Naguib, V.N. Mochalin, Y. Dall’Agnese, M. Heon, M.W. Barsoum, Y. Gogotsi, *Nat. Commun.* 4 (2013) 1–7.
- [21] M. Naguib, R.R. Unocic, B.L. Armstrong, J. Nanda, *Dalt. Trans.* 44 (2015) 9353–9358.
- [22] K. Huang, Z. Li, J. Lin, G. Han, P. Huang, *Chem. Soc. Rev.* 47 (2018) 6889.
- [23] H. Wang, Y. Wu, J. Zhang, G. Li, H. Huang, X. Zhang, Q. Jiang, *Mater. Lett.* 160 (2015) 537–540.
- [24] J. Halim, S. Kota, M.R. Lukatskaya, M. Naguib, M. Zhao, E.J. Moon, J. Pitock, J. Nanda, S.J. May, Y. Gogotsi, *Adv. Funct. Mater.* 26 (2016) 3118–3127.
- [25] F. Zhao, Y. Yao, C. Jiang, Y. Shao, D. Barceló, Y. Ying, J. Ping, J. Hazard. Mater. 384 (2020) 121358.
- [26] Y. Zhang, X. Jiang, J. Zhang, H. Zhang, Y. Li, *Biosens. Bioelectron.* 130 (2019) 315–321.
- [27] J. Liu, X. Jiang, R. Zhang, Y. Zhang, L. Wu, W. Lu, J. Li, Y. Li, H. Zhang, *Adv. Funct. Mater.* 29 (2019) 1807326.
- [28] X. Zhu, B. Liu, H. Hou, Z. Huang, K.M. Zeinu, L. Huang, X. Yuan, D. Guo, J. Hu, J. Yang, *Electrochim. Acta* 248 (2017) 46–57.
- [29] S. Kumar, Y. Lei, N.H. Alshareef, M.A. Quevedo-Lopez, K.N. Salama, *Biosens. Bioelectron.* 121 (2018) 243–249.
- [30] R.B. Rakhi, P. Nayak, C. Xia, H.N. Alshareef, *Sci. Rep.* 6 (2016) 1–10.
- [31] C. Dincer, R. Ktaich, E. Laubender, J.J. Hees, J. Kieninger, C.E. Nebel, J. Heinze, G.A. Urban, *Electrochim. Acta* 185 (2015) 101–106.
- [32] M. Stoytcheva, R. Zlatev, Z. Velkova, V. Gochev, G. Montero, L. Toscano, A. Olivas, *Curr. Anal. Chem.* 13 (2017) 89–103.
- [33] D. Lakshmi, M.J. Whitcombe, F. Davis, P.S. Sharma, B.B. Prasad, *Electroanalysis* 23 (2011) 305–320.
- [34] M.M. Rahman, N.S. Lopa, M.J. Ju, J.J. Lee, *J. Electroanal. Chem.* 792 (2017) 54–60.
- [35] D. Jin, M.H. Seo, B.T. Huy, Q.T. Pham, M.L. Conte, D. Thangadurai, Y.I. Lee, *Biosens. Bioelectron.* 77 (2016) 359–365.
- [36] M. Mesias-Garcia, E. Guerra-Hernandez, B. Garcia-Villanova, *J. Agric. Food Chem.* 58 (2010) 6027–6032.
- [37] R. Jerome, A.K. Sundramoorthy, *J. Electrochem. Soc.* 166 (2019) B3017–B3024.
- [38] G.V. Rebec, R.C. Pierce, *Prog. Neurobiol.* 43 (1994) 537–565.

- [39] N. Moghimi, K.T. Leung, *Anal. Chem.* 85 (2013) 5974–5980.
- [40] Q. Zhu, J. Bao, D. Huo, M. Yang, C. Hou, J. Guo, M. Chen, H. Fa, X. Luo, Y. Ma, *Sensors Actuat. B: Chem.* 238 (2017) 1316–1323.
- [41] C.L. Sun, H.H. Lee, J.M. Yang, C.C. Wu, *Biosens. Bioelectron.* 26 (2011) 3450–3455.
- [42] C. Wang, J. Du, H. Wang, C. Zou, F. Jiang, P. Yang, Y. Du, *Sensors Actuat. B: Chem.* 204 (2014) 302–309.
- [43] Z.H. Sheng, X.Q. Zheng, J.Y. Xu, W.J. Bao, F.B. Wang, X.H. Xia, *Biosens. Bioelectron.* 34 (2012) 125–131.
- [44] J. Ping, J. Wu, Y. Wang, Y. Ying, *Biosens. Bioelectron.* 34 (2012) 70–76.
- [45] Q. Li, C. Huo, K. Yi, L. Zhou, L. Su, X. Hou, *Sensors Actuat. B: Chem.* 260 (2018) 346–356.
- [46] N. Murugan, M.B. Chan-Park, A.K. Sundramoorthy, *J. Electrochem. Soc.* 166 (2019) B3163–B3170.
- [47] N. Murugan, T.H.V. Kumar, N.R. Devi, A.K. Sundramoorthy, *New J. Chem.* 43 (2019) 15105–15114.
- [48] W. Zhang, Y. Chai, R. Yuan, J. Han, S. Chen, *Sensors Actuat. B: Chem.* 183 (2013) 157–162.
- [49] K. Ghanbari, N. Hajheidari, *Anal. Biochem.* 473 (2015) 53–62.
- [50] Y.J. Yang, W. Li, *Biosens. Bioelectron.* 56 (2014) 300–306.
- [51] S. Wang, W. Zhang, X. Zhong, Y. Chai, R. Yuan, *Anal. Methods* 7 (2015) 1471–1477.
- [52] S. Mukdasai, U. Crowley, M. Pravda, X. He, E.P. Nesterenko, P.N. Nesterenko, B. Paull, S. Srijaranai, J.D. Glennon, E. Moore, *Sensors Actuat. B: Chem.* 218 (2015) 280–288.
- [53] X. Zhang, Y.C. Zhang, L.X. Ma, *Sensors Actuat. B: Chem.* 227 (2016) 488–496.
- [54] Y. Wen, T.E. Rufford, X. Chen, N. Li, M. Lyu, L. Dai, L. Wang, *Nano Energy* 38 (2017) 368–376.
- [55] D. Applestone, A. Manthiram, *RSC Adv.* 2 (2012) 5411–5417.
- [56] E. Restrepo, V. Benavides, A. Devia, S. Olarte, M. Arroyave, Y.C. Arango, *Brazil. J. Phys.* 34 (2004) 1748–1751.
- [57] V. Swamy, A. Kuznetsov, L.S. Dubrovinsky, R.A. Caruso, D.G. Shchukin, B.C. Muddle, *Phys. Rev. B* 71 (2005) 184302.
- [58] T. Hu, J. Wang, H. Zhang, Z. Li, M. Hu, X. Wang, *Phys. Chem. Chem. Phys.* 17 (2015)

9997–10003.

- [59] L. Zhang, W. Su, Y. Huang, H. Li, L. Fu, K. Song, X. Huang, J. Yu, C.T. Lin, *Nanoscale Res. Lett.* 13 (2018) 343.
- [60] M. Hu, T. Hu, Z. Li, Y. Yang, R. Cheng, J. Yang, C. Cui, X. Wang, *ACS Nano* 12 (2018) 3578–3586.
- [61] Y. Wen, T.E. Rufford, D. Hulicova-Jurcakova, X. Zhu, L. Wang, *ACS Appl. Mater. Interfaces* 8 (2016) 18051–18059.
- [62] Y. Tang, J. Zhu, W. Wu, C. Yang, W. Lv, F. Wang, *J. Electrochem. Soc.* 164 (2017) A923–A929.
- [63] C. Yang, W. Que, X. Yin, Y. Tian, Y. Yang, M. Que, *Electrochim. Acta* 225 (2017) 416–424.
- [64] X. Zhang, W. Yan, J. Zhang, Y. Li, W. Tang, Q. Xu, *RSC Adv.* 5 (2015) 65532–65539.
- [65] S.S. Shankar, R.M. Shereema, R.B. Rakhi, *ACS Appl. Mater. Interfaces* 10 (2018) 43343–43351.
- [66] J. Jiang, X. Du, *Nanoscale* 6 (2014) 11303–11309.
- [67] P. Gai, H. Zhang, Y. Zhang, W. Liu, G. Zhu, X. Zhang, J. Chen, J. Mater. Chem. B 1 (2013) 2742–2749.
- [68] N.M.M.A. Edris, J. Abdullah, S. Kamaruzaman, M.I. Saiman, Y. Sulaiman, *Arab. J. Chem.* 11 (2018) 1301–1312.
- [69] F. Li, J. Chai, H. Yang, D. Han, L. Niu, *Talanta* 81 (2010) 1063–1068.
- [70] X. Feng, Y. Zhang, J. Zhou, Y. Li, S. Chen, L. Zhang, Y. Ma, L. Wang, X. Yan, *Nanoscale* 7 (2015) 2427–2432.
- [71] V. Veeramani, R. Madhu, S.-M. Chen, B.-S. Lou, J. Palanisamy, V.S. Vasanth, *Sci. Rep.* 5 (2015) 10141.
- [72] B. Hu, Y. Liu, Z.W. Wang, Y. Song, M. Wang, Z. Zhang, C.S. Liu, *Appl. Surf. Sci.* 441 (2018) 694–707.
- [73] D. Zhao, G. Yu, K. Tian, C. Xu, *Biosens. Bioelectron.* 82 (2016) 119–126.
- [74] K.C. Lin, T.H. Tsai, S.M. Chen, *Biosens. Bioelectron.* 26 (2010) 608–614.
- [75] S. Yu, C. Luo, L. Wang, H. Peng, Z. Zhu, *Analyst* 138 (2013) 1149–1155.
- [76] S. Qi, B. Zhao, H. Tang, X. Jiang, *Electrochim. Acta* 161 (2015) 395–402.
- [77] A. Safavi, N. Maleki, O. Moradlou, F. Tajabadi, *Anal. Biochem.* 359 (2006) 224–229.

[78] L. Yang, D. Liu, J. Huang, T. You, Sensors Actuat. B: Chem. 193 (2014) 166–172.

Journal Pre-proof

Figure lists:

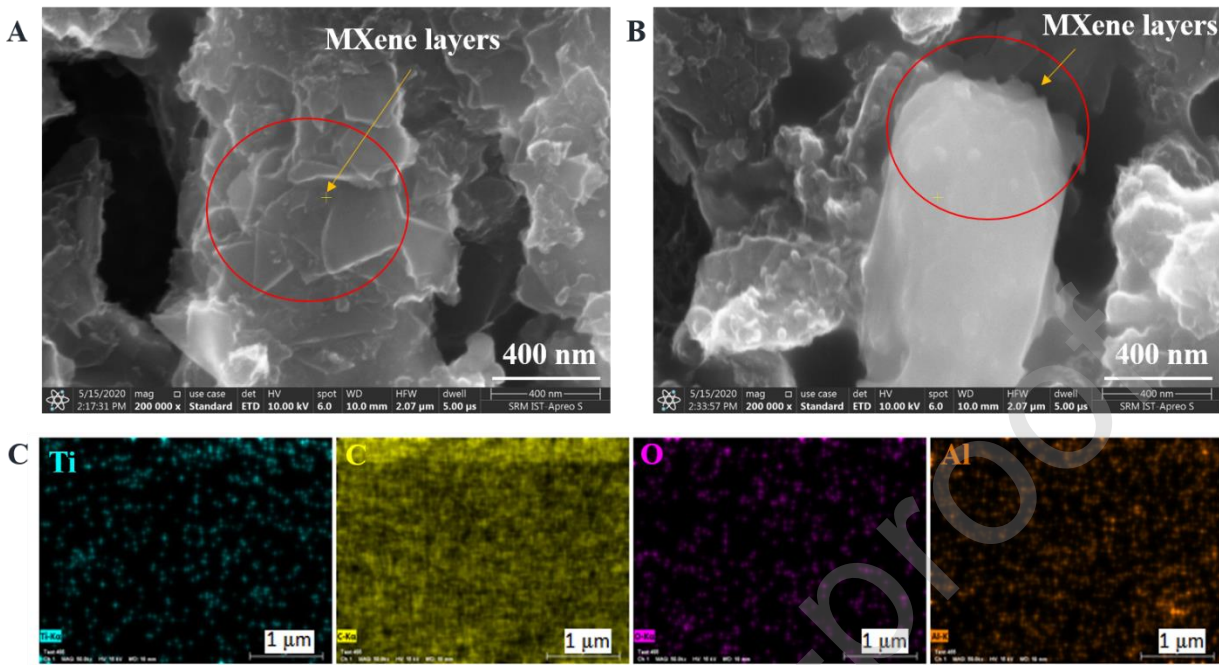


Fig. 1. (A, B) HR-SEM images of the mixed phase Ti-C- T_x (MXene) layered materials and (C) EDS mapping of Ti, C, O and Al.

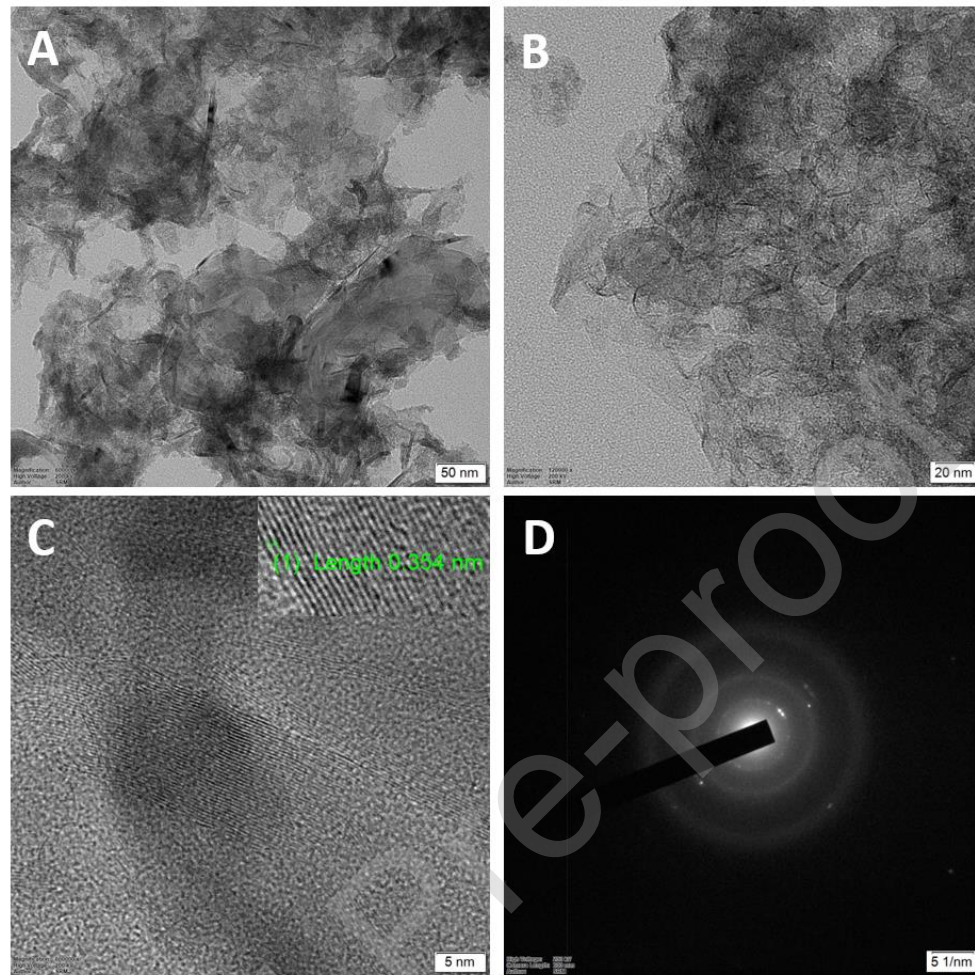


Fig. 2. (A, B) TEM images of the Ti-C- T_x nanosheets with different magnifications, (C) HR-TEM images of Ti-C- T_x layers and (D) SAED pattern of Ti-C- T_x layers.

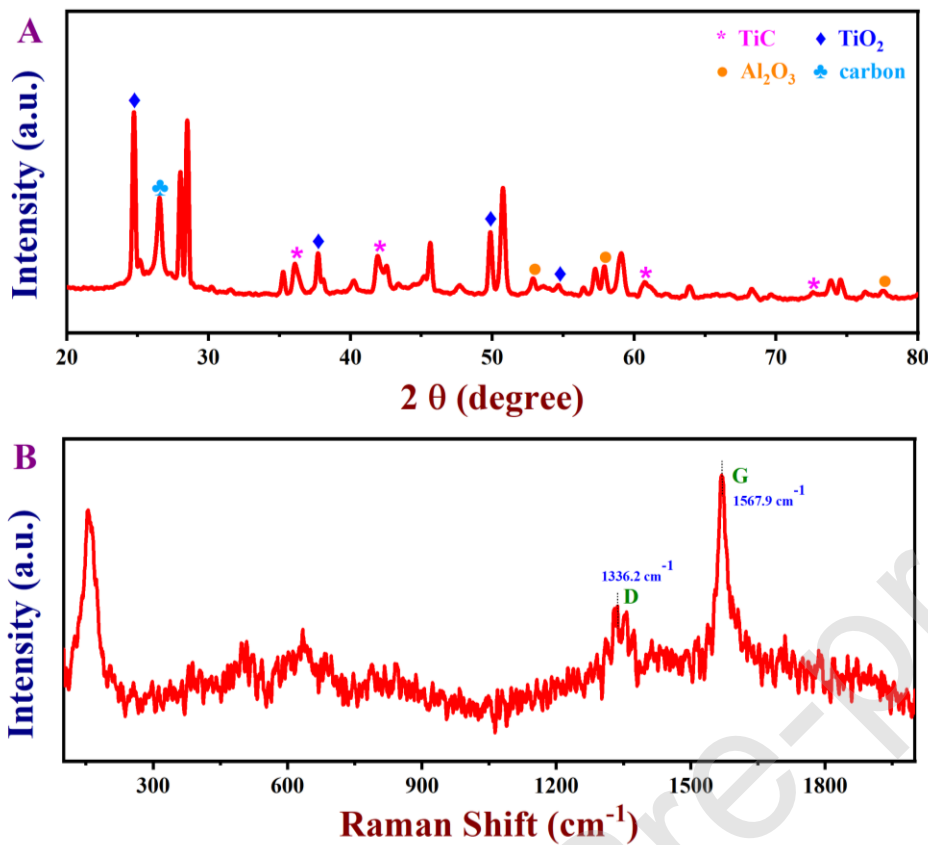


Fig. 3. (A) XRD pattern of mixed phase titanium carbide (Ti-C-T_x) MXnene nanosheets and (B) Raman spectrum of mixed phase titanium carbide (Ti-C-T_x) layered material (532 nm laser was used).

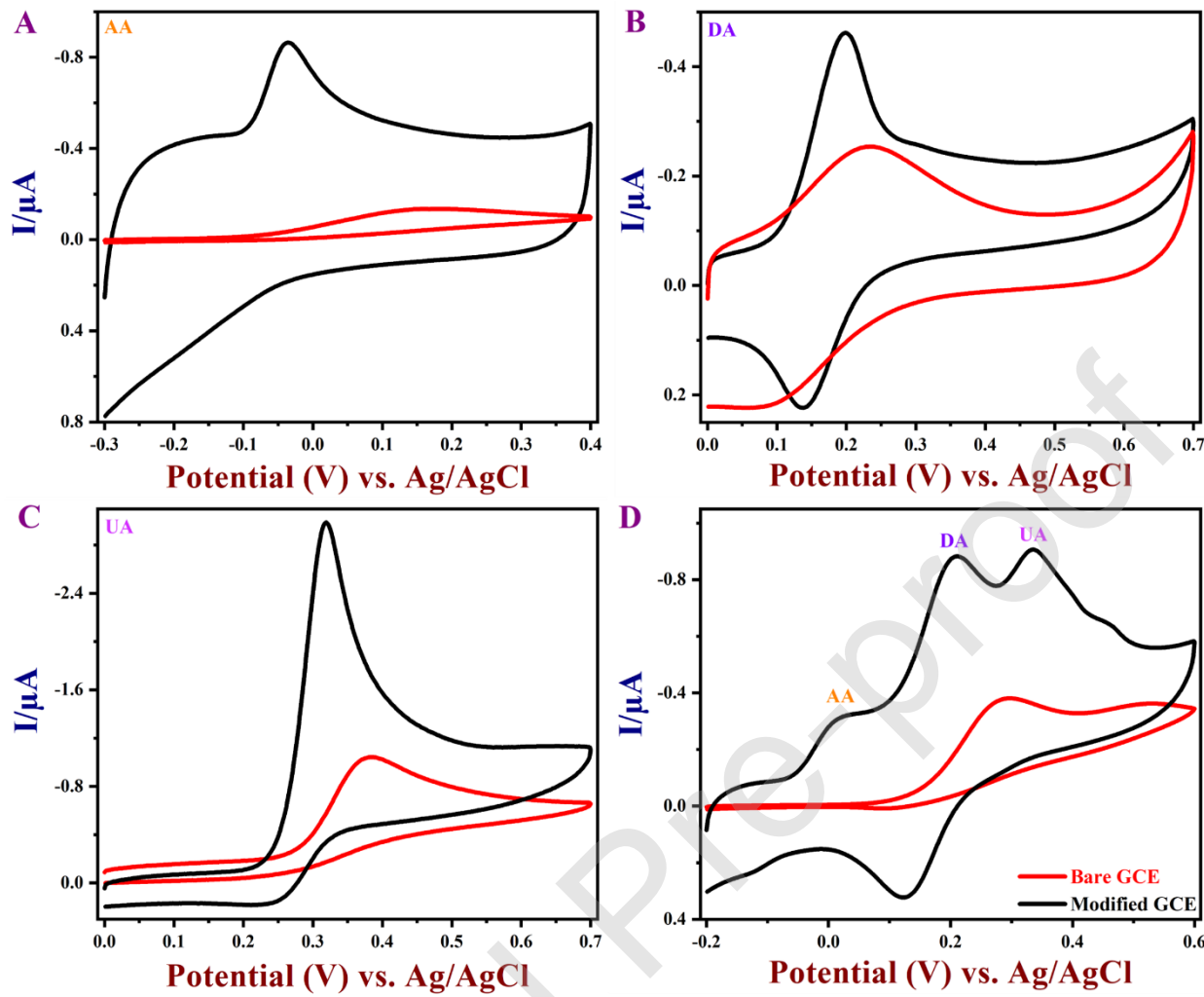


Fig. 4. Cyclic voltammograms (CVs) recorded using a bare GCE (red), and Ti-C-T_x/GCE (black) in (A) 1 mM AA, (B) 1 mM DA, (C) 1 mM UA and (D) mixture of 1 mM of (AA, DA and UA) + 0.1 M PBS (pH 7.4).

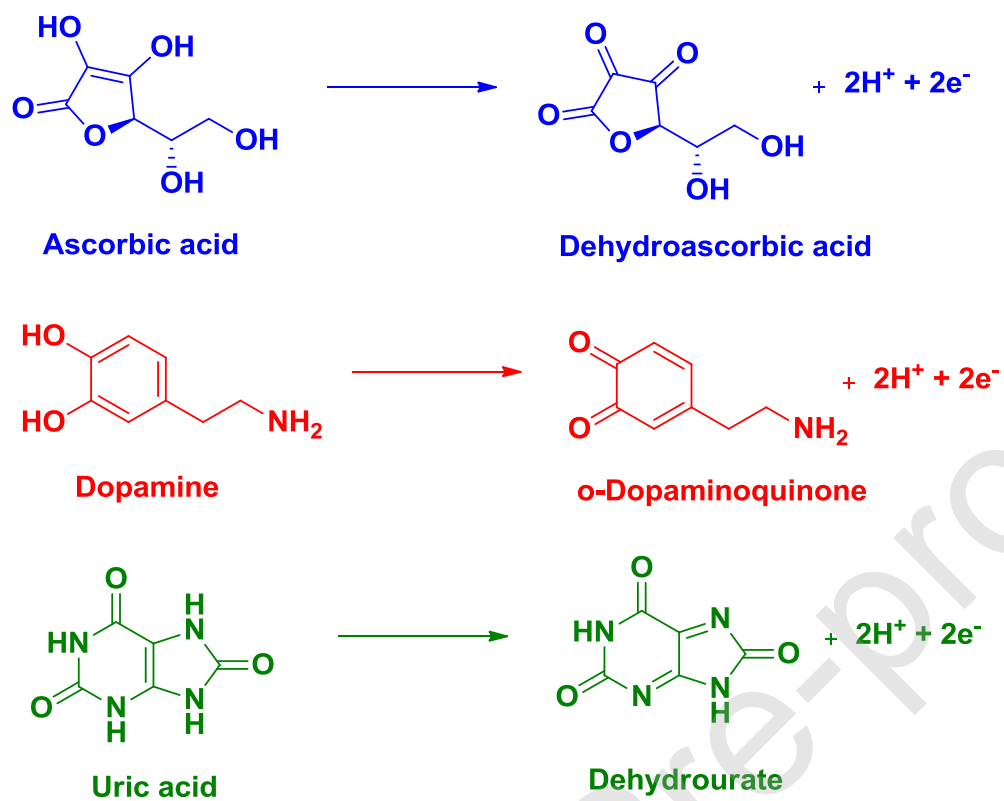


Fig. 5. The electro-oxidation reaction mechanisms of AA, DA and UA at Ti-C-T_x/GCE.

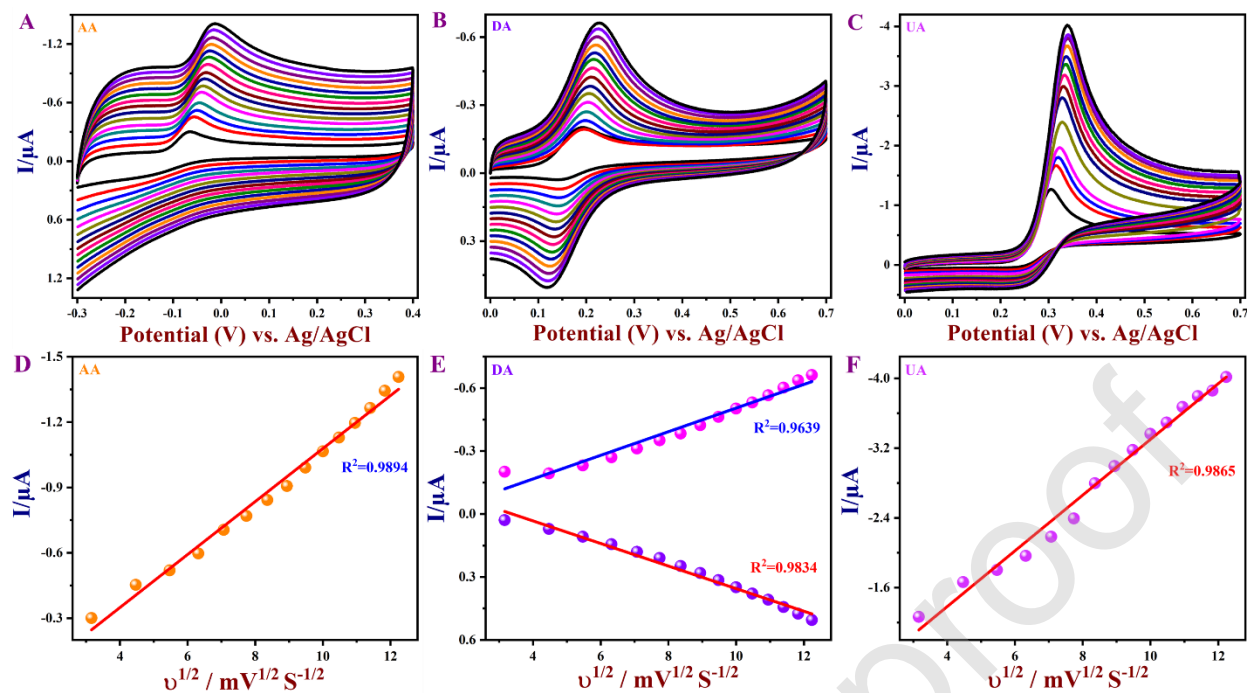


Fig. 6. The CVs of Ti-C- T_x /GCE electrode recorded in (A) 1 mM AA, (B) 1 mM DA, (C) 1 mM UA at different scan rates in the range from 10 to 150 mV s⁻¹, respectively. (D-F) The linear plots of AA, DA and UA obtained from their oxidation peak current *vs.* square-root of the scan rates.

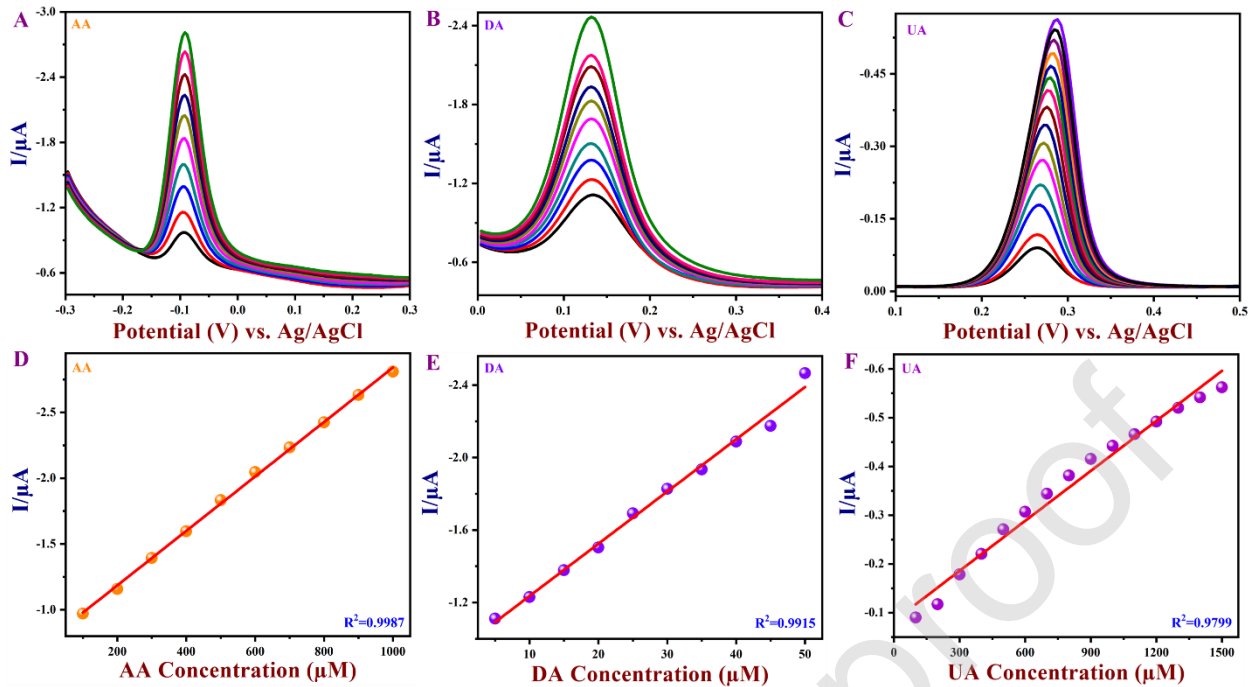


Fig. 7. (A, B, C) DPVs recorded for different individual concentrations of AA, DA and UA at the Ti-C-T_x/GCE in 0.1 M PBS (pH 7.4) upon successive additions of different concentrations from 100 to 1000 μM for AA, 5 to 50 μM for DA and 100 to 1500 μM for UA, respectively. (D, E, F) The calibration curves made for AA, DA and UA using their concentrations vs. oxidation peak currents.

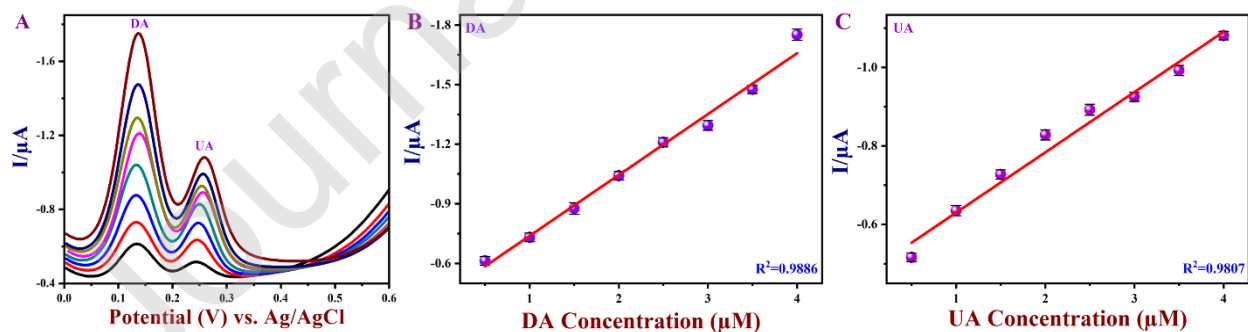


Fig. 8. (A) DPVs recorded for different concentrations of DA and UA at the Ti-C-T_x/GCE in 0.1 M PBS (pH 7.4) with successive additions from 0.5 to 4 μM for DA and 0.5 to 4 μM for UA,

respectively. (B, C) The calibration curves made from the oxidation peaks currents against concentration of DA and UA, respectively.

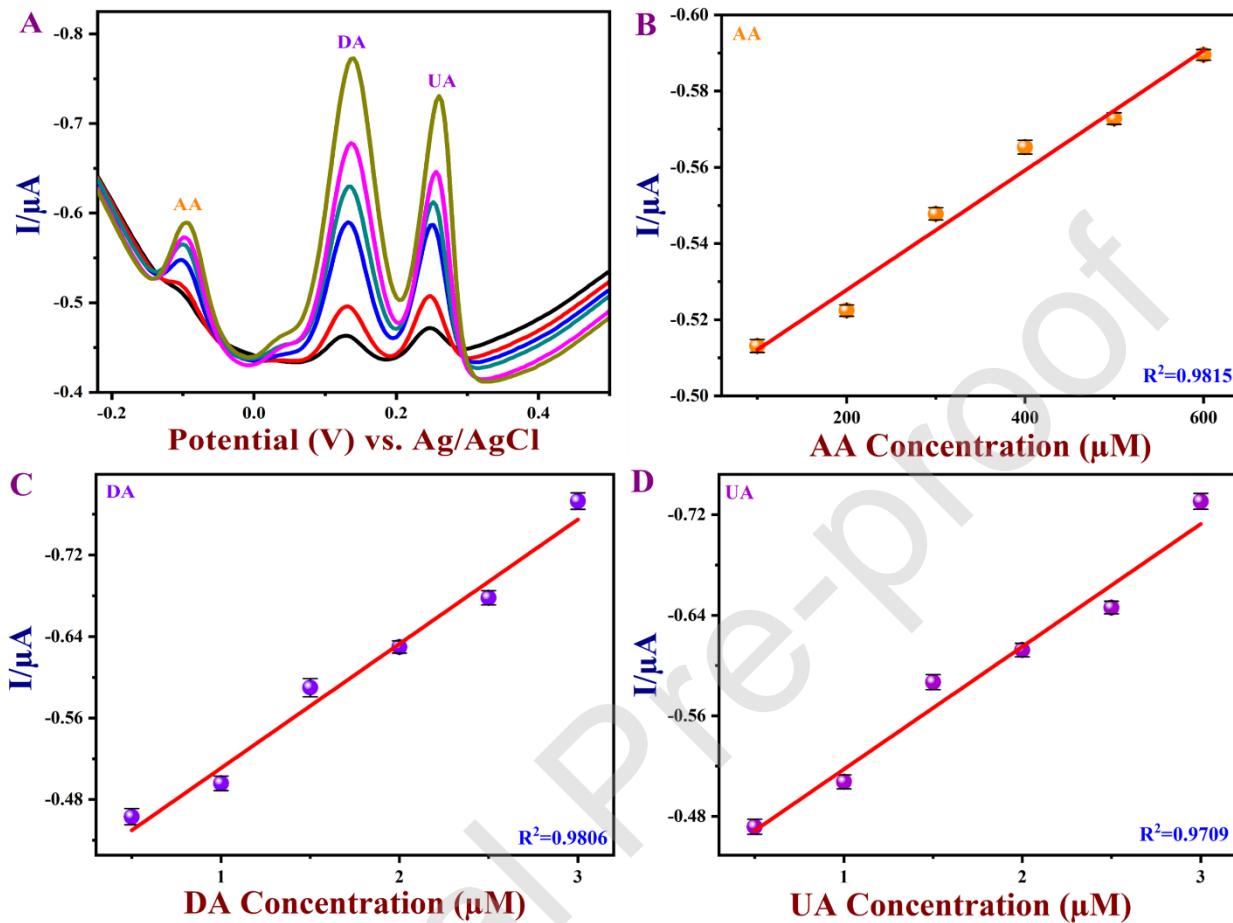


Fig. 9. (A) DPVs recorded for different concentrations of AA, DA and UA at the Ti-C-T_x/GCE in 0.1 M PBS (pH 7.4) upon successive additions from 100 to 600 μM for AA, 0.5 to 3 μM for DA and 0.5 to 3 μM for UA, respectively. (B-D) The calibration curves made for AA, DA and UA from their oxidation peak currents vs. concentrations.

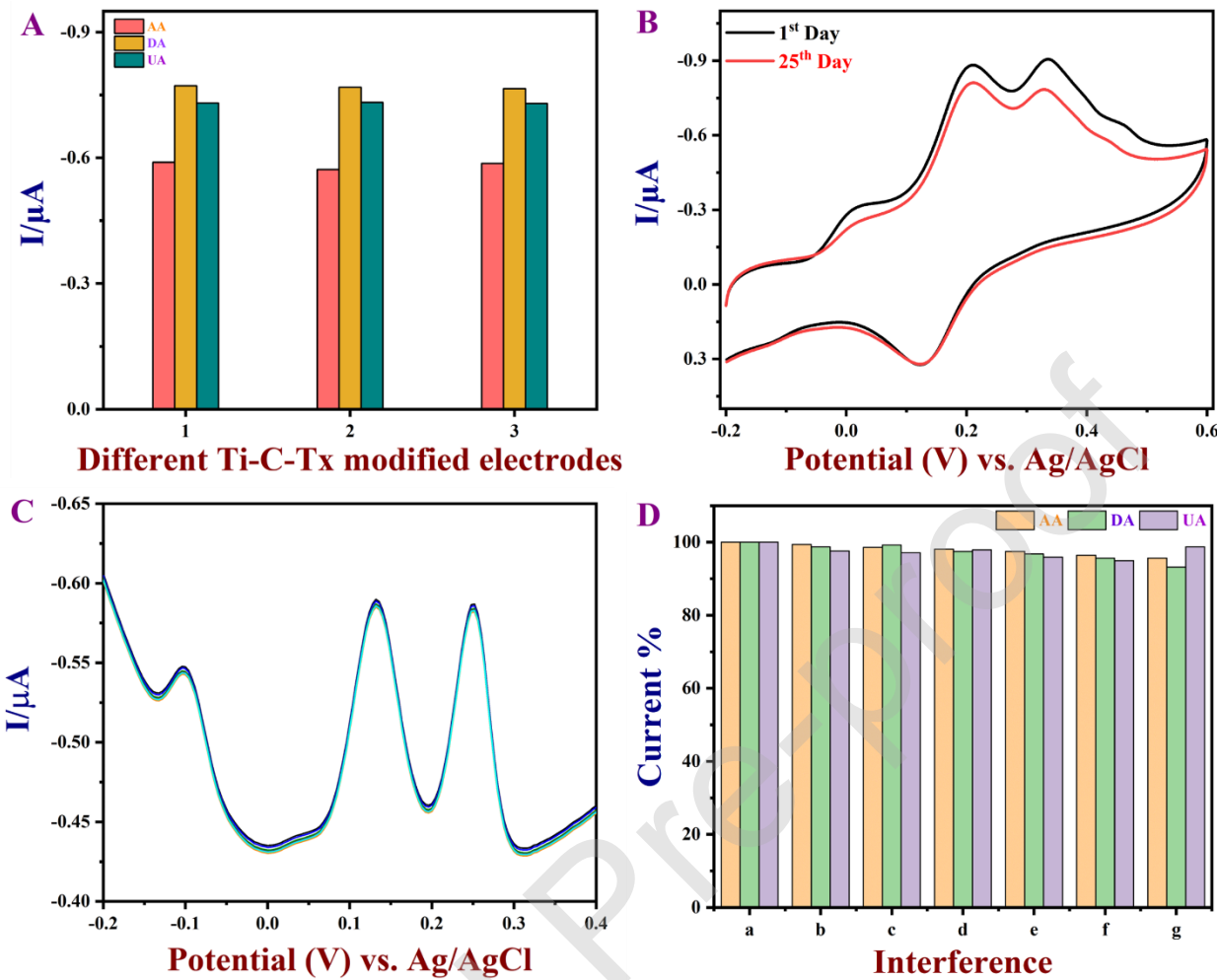
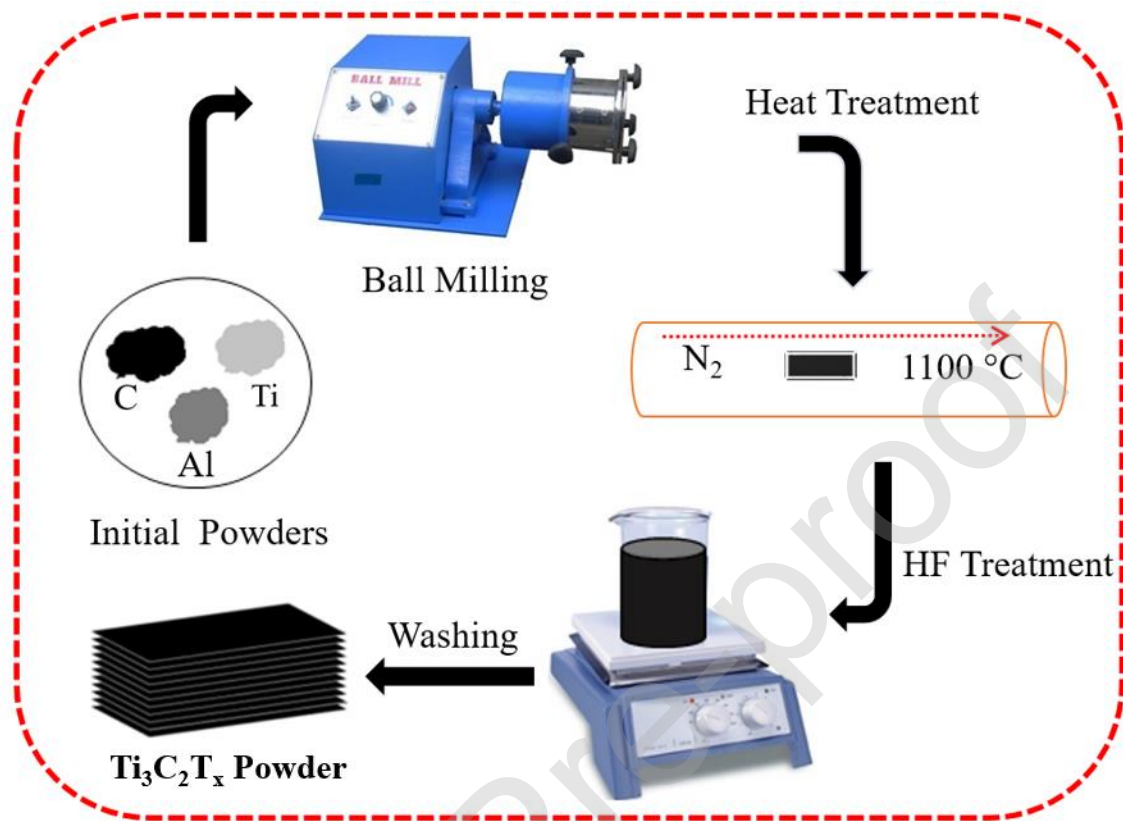


Fig. 10. (A) DPV response of three different Ti-C-T_x modified electrodes were investigated at fixed concentrations of AA, DA and UA (each 1 mM) in PBS. (B) CVs of $\text{Ti-C-T}_x/\text{GCE}$ in 0.1 M PBS (pH 7.4) containing AA, DA and UA (1 mM) after several days of storage. (C) DPV responses were recorded using of $\text{Ti-C-T}_x/\text{GCE}$ in 0.1 M PBS containing AA (300 μM), DA (1.5 μM), UA (1.5 μM) with the presence of 10 fold concentrated interferent molecules. (D) Histogram representing the variation of peak current responses with the addition of interferent molecules such as (b) urea (c) nicotine, (d) l-cysteine, (e) paracetamol, (f) Cd^{2+} and (g) Pb^{2+} in the presence of (a) AA, DA and UA.



Scheme 1. Schematic illustration for the preparation of $\text{Ti}_3\text{C}_2\text{T}_x$ powders.

Table 1 Analytical data comparison between proposed method and other reported sensors for electrochemical simultaneous detection of AA, DA and UA.

Electrode materials	Linear range (μM)			Limit of detection (LOD) (μM)			Refs.
	AA	DA	UA	AA	DA	UA	
AC/GCE	30–95	1–65	2–230	4.96	0.06	0.75	[71]
Fe ₃ O ₄ /Co ₃ O ₄ /mC@g-C ₃ N ₄ /GCE	500–8000	1–70	5–100	12.55	0.21	0.18	[72]
HNP-PtTi	200–1000	4–500	100–1000	24.2	3.2	5.3	[73]
GO/MWNT	5.0–300	5.0–500	3.0–60	1.0	1.5	1.0	[50]
MWCNT-PEDOT/GCE	100–2000	10–330	10–250	100	10	10	[74]
PEDOT-modified Ni/Si MCP	20–1400	12–48	36–216	10	1.5	2.7	[75]
PG/GCE	9–2314	5–710	6–1330	6.45	2.00	4.82	[76]
CILE	50–7400	2–1500	2–220	20	1.00	1.00	[77]
ERGO/GCE	500–2000	0.5–60	0.5–60	250	0.5	0.5	[78]
Ti-C-T _x /GCE	100–1000	0.5 – 50	0.5 – 4; 100 – 1500	4.64	0.06	0.075	This work

Footnotes: (AC) - activated carbon, (GCE)-Glassy carbon electrode, (mC)-Mesoporous carbon, (g-C₃N₄)-graphitic carbon nitride, (Fe₃O₄)-Iron oxide, (Co₃O₄)-Cobalt oxide, (HNP)- Hierarchical nanoporous, (PtTi)-(Platinum titanium) (PEDOT)-Poly(3,4-ethylenedioxythiophene), (GO)-Graphene oxide (MWNTs)-Multiwalled carbon nanotubes, (Ni/Si MCP)-Ni/silicon microchannel plate, (PG)-Pristine graphene, (CILE)-Carbon ionic liquid electrode and (ERGO)- Electrochemically reduced graphene oxide.

Table 2 DPV analysis of spiked AA, DA and UA in diluted human urine samples using Ti-C-T_x modified GCE as a sensor (*n*=3).

Sample	Analyte	Concentration added (μM)	Found (μM)*	Recovery (%)
Urine	AA	100	102 ±1.1	101
	DA	20	20.1 ± 0.6	100.5
	UA	100	103 ± 1.3	103

*Mean of three measurements.